Pivot-based Collective Coverage Control with a Multi-robot Team

Shaocheng Luo, Jun Han Bae, and Byung-Cheol Min

***Abstract*— This paper presents a novel collective coverage control strategy for robots to achieve effective coverage over a large-scale spill. The proposed idea is based on the divide and conquer approach that partitions a large irregular spill in the workspace into a number of smaller zones and let the robot team cover each packing zone sequentially. Ultimately, the robot team can cover the entire area. For an effective coverage operation in diverse and dynamic environments, we propose a pivot-based control strategy performed by a pivot robot and multiple planet robots. The pivot robot is located at the center of the area to be covered and serves as a lighthouse to all the working robots denoted as planet robots exploring the area. By doing so, the planet robots do not require a global coordinate system nor massive communication between robots for their coordination, ultimately enabling an efficient, adaptive, scalable, and fault tolerant coverage operation. The proposed strategy is validated through extensive simulation experiments with different packing shapes and different numbers of robots.**

***Keywords*— Coverage Control, Multi-Robot Coordination, Networked Robots, Artificial Potential Field.**

I. INTRODUCTION

Coverage problems for mobile robots have been studied for a long time due to their wide and various applications such as oil spills cleaning [1]. However, many past researches have been limited to a single-robot scenario which is inferior in coverage efficiency and unconducive to large-scale situations [2]. Recently, coverage control using multi-robot systems to increase the coverage efficiency has been actively pursued [3]. However, high efficient, scalable, and fault tolerant coverage strategies for diverse and dynamic environments have not yet been fully discovered due to the challenges of coordination and communication among robots. Moreover, research is also underway to handle various workspace shapes and large-scale coverage problems, but the results are unsatisfactory.

In this paper, we propose a new collective operation control strategy with the advantages including high efficiency, strong scalability, fault tolerance, and unknown obstacle avoidance. This strategy first uses the divide and conquer approach and partitions a large-scale irregular spill into multiple small areas with certain basic geometric shapes, such as squares, triangles, hexagons, and circles. The partition process is also named as geometric packing or tessellation [4]. Then, using the proposed strategy, the robot team consisting of a pivot robot and multiple plant robots will cover each packing area sequentially and ultimately enables a fully coverage to the entire workspace. Fig. 1 illustrates the proposed collective coverage control strategy. The pivot robot

S. Luo, J. Bae, and B.-C. Min are with SMART Lab, Department of Computer and Information Technology, Purdue University, West Lafayette, IN 47907, United States. {luo191,bae21,minb}@purdue.edu

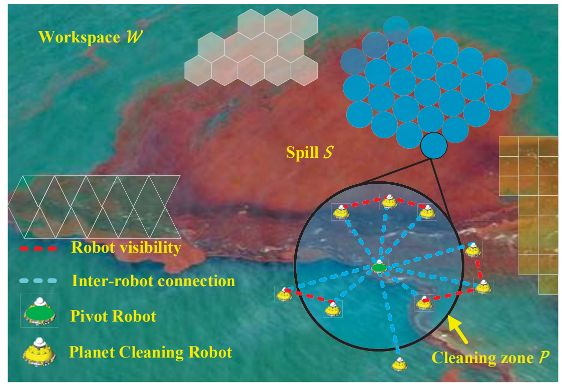

Fig. 1: An image that illustrates our proposed collective coverage strategy for various geometric packing shapes, including circles, squares, triangles, and hexagons for irregular spill coverage. Blue dashline shows the connectivities between planet robots (yellow) and the pivot robot (green). Red dashline represents one robot being in the vision of another robot. (Photo credit to *Smithsonian.com*)

is located at the center of the area to be covered and serves as the lighthouse to all working robots denoted as planet robots. Planet robots are connected wirelessly with the pivot robot. The planet robot determines its movement by referencing the estimated relative location of the pivot robot via radio signal strength measurement [5], [6] and uses an on-board vision sensor [7] to detect the spill boundary and avoid the collision with other robots. In this way, the planet robot does not require massive communication among the robots nor a global coordinate system, but the whole team ultimately enables an effective and efficient coverage operation.

The proposed coverage control strategy is verified by extensive simulation experiments using different packing types and different numbers of robots.

II. PROBLEM STATEMENT AND PROPOSED APPROACH

In this section, we state our research question based on assumptions. Then, we elaborate on the coverage model with moving robots and provide the control algorithm to achieve the complete coverage over a large-scale spill. The control algorithm features pivot-based multi-robot coordination and collision avoidance between robots.

A. Problem Statement and Assumptions

Assume the spill is static, and its packing areas are available after geometric packing process. We propose our research question to be: How a team of robots can collectively clean up a packing area with only local sensing but not a global coordinate frame or external positioning device? Specifically, the whole spill in the workspace $\mathcal{W} \in \mathbb{R}^2$ is

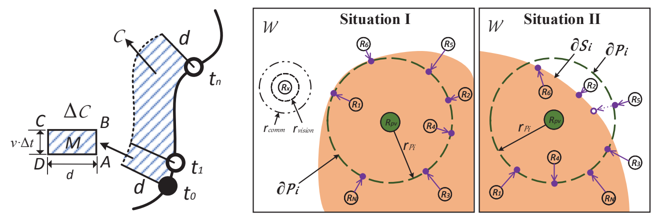

(a) (b)

Fig. 2: (a) Coverage manifold when a robot maneuvers along $\mathcal{S}_i$. An approximated fractional coverage area after Δt time with speed v is shown as $\Delta\mathcal{C}$. (b) Two possible situations in coverage operation under circular packing. $\partial\mathcal{P}$ and $\partial\mathcal{S}$ represent the boundaries of the packing area and the spill, respectively. Pivot robot R_{pv} (green) is located at centroid of the packing area. r_{vision} and r_{comm} denote the vision sensor and wireless connection ranges for planet robots. The purple dots indicate the deployment goals for planet robots.

denoted as $\mathcal{S}_\mathcal{W} \in \mathbb{R}^2$. The packing areas after the geometric packing are denoted as below,

$$\mathcal{P}_i = \{(x, y) : (x, y \in interior(PP_x)_i)\}, \forall i = 1, ..., \mathtt{M}, \quad (1)$$

where PP_x stands for a specific *packing pattern* such as circle, triangle, square, or hexagon; $\mathtt{M}$ denotes the total number of packing areas for spill $\mathcal{S}_\mathcal{W}$. Since the spill remained in the packing area $\mathcal{P}_i$ is changing because of on-going cleanup, we define it as:

$$\mathcal{S}_i = \{(x, y) : (x, y \in interior(PP_x)_i) \cap (x, y \in \mathcal{S}_\mathcal{W})\}, \quad \forall i = 1, ..., \mathtt{M}. \quad (2)$$

We use $\partial\mathcal{P}_i$ and $\partial\mathcal{S}_i$ to denote the boundary of $\mathcal{P}_i$ and $\mathcal{S}_i$, respectively. If $\partial\mathcal{S}_i$ does not exist or is not closed initially since $\mathcal{S}_i \nsubseteq \mathcal{P}_i$, the control algorithm should enable robots to create a closed boundary $\partial\mathcal{S}_i$ such that $\mathcal{S}_i \subseteq \mathcal{P}_i$. In this case, robots can track the spill boundary $\partial\mathcal{S}_i$ and realize complete coverage over $\mathcal{S}_i$.

We further state the following assumptions that our research is based on: The spill to be covered is overall integrated and has a smooth boundary; the spill is featured by colors or textures that can be distinguished from the base using image processing techniques.

B. Pivot-based Coverage Control Strategy

The coverage operation starts when the packing process is completed. The targeted large-scale spill is partitioned into $\mathtt{M}$ number of small packing areas with specific shapes, note that the centroid of the packing area should reside in $\mathcal{S}_i$. Meanwhile, the radius of the packing area cannot exceed the range of wireless connectivity, i.e., $r_{\mathcal{P}i} \leq r_{comm}$. Otherwise, the planet robots may not be able to identify the pivot robot and localize itself. We first deploy the pivot robot to the centroid[1] of the first packing area $\mathcal{S}_1$. The pivot robot can be randomly selected and it can move autonomously to the designated position under operator's guidance. The planet robots start performing coverage after the pivot robot is ready. The connectivity can be built between the planet robot to the pivot robot by simply using a paired Wi-Fi Access Point (AP) (for pivot robot) and an adapter combined with an antenna (for planet robot). We can localized the planet robot, including bearing and distance, through Wi-Fi signal strength of the pivot robot [5], [8].

We show the coverage model here. When a robot is maneuvering in $\mathcal{S}_i$ and traveled points A(x_1, y_1) and B(x_2, y_2) in sequence, the coverage manifold can be formulated as:

$$\Delta\mathcal{C} = \{\mathrm{M}(x, y) : (0 < \mathbf{AM} \cdot \mathbf{AB} < \mathbf{AB} \cdot \mathbf{AB}) \cap (0 < \mathbf{AM} \cdot \mathbf{AD} < \mathbf{AD} \cdot \mathbf{AD})\}, \quad (3)$$

$$\mathrm{D}(x_4, y_4) = \Big(-\sqrt{\|\mathbf{AD}\|^2 - y_4^2}\,,\ \frac{\|\mathbf{AB}\|^2 + \|\mathbf{AD}\|^2 - \|\mathbf{BD}\|^2}{2\|\mathbf{AD}\|}\Big) \quad (4)$$

where M is a point in $\Delta\mathcal{C}$, and $\|\mathbf{AD}\| = d$ is the horizontal coverage distance. The coverage manifold is demonstrated in Fig. 2a. Furthermore, assuming a maximal processing capacity $\mathcal{V}$ of a robot in removing the spill, such as the centrifugal volume to algae spill harvesting and the filtering system capacity to oil spill cleaning, by having $\Delta\mathcal{C} = vd\Delta t = \mathcal{V}\Delta t$, the maximum speed of the robot is bounded by $\dot{q}_{max} = \frac{\mathcal{V}}{d}$.

The coverage model (3) can be interpreted as the robot cleans the spill d distance to its left during maneuvering. This model can be applied in existing robots such as [9]. Note d value relies on the curvature of the trajectory, and can be approximated based on the contour of the spill. We choose left hand side coverage for the purpose that we want all the robots to travel uniformly counterclockwise to avoid the collision and realize a distributed coverage behavior. The details will be elaborated later.

Now we provide the coverage control algorithm that enables a full coverage to the packing area to remove the spill, and converges to the pivot when the operation reaches an end. Using $\mathbf{q}_i = (x_i, y_i)$ and $\mathbf{q}_{pv} = (x_{pv}, y_{pv})$ to denote the position of a planet robot R_i and the pivot robot R_{pv}, and $r_{\mathcal{P}j}$ to denote the radius of packing area $\mathcal{P}_j$, Algorithm 1 shows the procedure of the coverage control that runs iteratively until the operation is completed.

To illustrate Algorithm 1, we present a finite state transition diagram consisting of *four* states in Fig. 3. Meanwhile, we sketch two possible initial situations under circular packing with randomly distributed robots in Fig. 2b. In the transition diagram, every robot starts with deployment (*State 1*), where it moves toward the goal position on $\partial\mathcal{P}_j$. Especially, if the robot experiences a traverse $\mathcal{S}_j \rightarrow \neg\mathcal{S}_j$, it stops at the traverse point on $\partial\mathcal{S}_j$ and terminates deployment. This case is demonstrated by R_6 in Situation II of Fig. 2b. *State 2* means if the robot is deployed but does not detect $\partial\mathcal{S}_j$ or reside in $\mathcal{S}_j$, it will start moving toward the pivot robot until it detects $\partial\mathcal{S}_j$. This state is demonstrated by R_5 in Situation II. Note that the robot can travel as fast as it can in *State 1 and 2*, since it is not performing the coverage. In *State 3*, if no $\partial\mathcal{S}_j$ is detected but the robot resides in the spill, it will maneuver along $\partial\mathcal{P}_j$ and create a boundary $\partial\mathcal{S}_j$

[1] In fact, the pivot robot can be at any place within $\mathcal{S}_i \cap \mathcal{P}_i$ in certain circumstances such as $\mathcal{S}_i \subseteq \mathcal{P}_i$. Here, we assume the pivot to be the centroid of $\mathcal{P}_i$ just to simplify the analysis.

Algorithm 1: Collective Coverage Control Algorithm for every planet robot in packing area $\mathcal{P}_j$

repeat
  for R_i under deployment (State 1) **do**
    R_i moves from $\mathbf{q}_i$ to $\mathbf{q}_{vt} + \frac{\mathbf{q}_i - \mathbf{q}_{pv}}{\|\mathbf{q}_i - \mathbf{q}_{pv}\|} r_{\mathcal{P}j}$;
    if R_i experiences a traverse $\mathcal{S}_j \to \neg\mathcal{S}_j$ **then**
      R_i stops at $\partial\mathcal{S}_j$;
  for R_i under coverage operation **do**
    if No $\partial\mathcal{S}_j$ is detected within r_{vision} **then**
      if R_i resides in $\mathcal{S}_j$ **then**
        R_i covers the spill under (3) by tracking $\partial\mathcal{P}_j$ and hence creates $\partial\mathcal{S}_j$ (State 3);
      else
        R_i moves toward $\mathbf{q}_{pv}$ (State 2);
    else if $\partial\mathcal{S}_j$ is detected within r_{vision} **then**
      R_i covers the spill under (3) by tracking $\partial\mathcal{S}_j$ (State 4);
      if $\|\mathbf{q}_i - \mathbf{q}_{pv}\| \geq r_{\mathcal{P}i}$ **then**
        R_i switches to track $\partial\mathcal{P}_j$ and continues the coverage operation (State 3);
    else
      R_i fails in vision sensing, it stops and becomes an obstacle;
    Bounding speed $\dot{q}_i = \frac{\nu}{d}$;
until $\|\mathbf{q}_i - \mathbf{q}_{pv}\| \leq \epsilon$, $\forall i \in \{1, ..., N\}$;

that trailing robots can follow in *State 4*. All the robots in Situation I and robots R_1, R_3, R_4, and R_N in Situation II demonstrate *State 3*, while R_2 and R_6 in Situation II demonstrate *State 4*. The coverage of this packing area ends up with all planet robots gathering around the pivot robot within a threshold ϵ according to the robot dimensions.

C. Motion Control based on Artificial Potential Field

To motivate robots to track $\partial\mathcal{S}_i$ or $\partial\mathcal{P}_i$ in order to cover the spill collectively but avoid collision, we introduce artificial potential field based motion controllers for each state. To avoid local minima and deadlock, we propose a pre-prioritized collision avoidance strategy to coordinate the robots working in different states. Meanwhile, all the robots performing coverage over the spill shall move counterclockwise (CCW) about the pivot robot when tracking $\partial\mathcal{S}_i$ or $\partial\mathcal{P}_i$. A uniform moving direction leads to a distributed coordinate control.

The proposed avoidance priority is indicated in Fig. 3, the robots working in lower priority have to yield to those working in higher priority, and robots performing the coverage have the highest priority. The avoidance priority for these states are determined as *3 = 4 > 1 = 2*. No transition exists between *State 2* and *State 3*, because the robot converges to the pivot only if nothing is detected. Furthermore, special consideration should be given to the robots working in the states of the same priority. As we stated above, robots working in *State 3* and *4* (i.e., tracking either $\partial\mathcal{S}_i$ or $\partial\mathcal{P}_i$) are moving uniformly CCW. Given a continuous and smooth spill boundary consisting of $\partial\mathcal{S}_i$ and $\partial\mathcal{P}_i$, the collision happens only between a leading robot and its trailing robot.

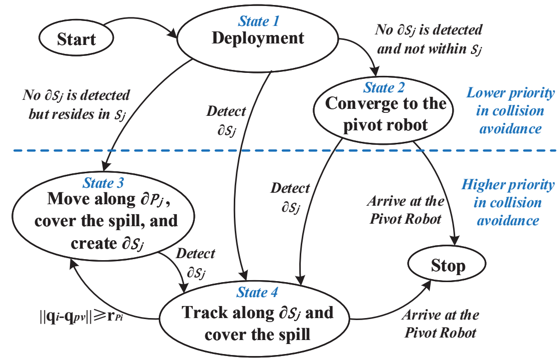

Fig. 3: A finite-state machine diagram showing the hybrid robot coordination strategy. The robots perform collective coverage over the spill when it is moving along either $\partial\mathcal{S}_j$ or $\partial\mathcal{P}_j$, i.e., *State 3* and *State 4*, which are of higher priority than the others in terms of collision avoidance.

However, the robot working in *State 3* does not have a leading or trailing robot, hence, we will limit the possible collisions to be from the robots working in *State 4*.

Similarly, for the robots working in *State 1* and *2*, since they are moving either towards or against the pivot robot, no collision is foreseen if their trajectories are non-coincident. Such a pre-prioritized collision avoidance rule eliminates local minima which halting the robot, and relies only on local sensing. In terms of deadlock, although not observed in the validation experiments, it can be tackled with appropriate motion planning methods [10]. In practice, robots can recognize each other's states with minimum communication or via light signals and near field communication such as Radio Frequency Identification (RFID) [11].

Assuming a single integrator model for planet robot control, i.e.,

$$\dot{\mathbf{q}}_i(t) = \mathbf{u}_i(t), \; i \in 1, ..., N \tag{5}$$

where $\mathbf{u}_i(t) \in \mathbb{R}^2$ denotes the control input for planet robot R_i at time instant t, the detailed motion control law for every state is provided below from Sec. II-C.1 to Sec. II-C.4.

1) Motion Controller for State 1: For robots working in *State 1*, provided the goal positions for deployment $\mathbf{q}_g = \mathbf{q}_{vt} + \frac{\mathbf{q}_i - \mathbf{q}_{pv}}{\|\mathbf{q}_i - \mathbf{q}_{pv}\|} r_{\mathcal{P}j}$, we construct an attractive potential field formulated as

$$U_d^{(1)}(\mathbf{q}) = \frac{1}{2}\xi_1 \|d(\mathbf{q}, \mathbf{q}_g)\|_2^2 \tag{6}$$

where ξ_1 is a scaling parameter and $\|d(\mathbf{q}, \mathbf{q}_g)\|_2$ is the distance between the current positions of robots and their goals obtained from radio signal strength measurement [5].

Additionally, we propose a repulsive potential exerted on the robots to avoid the collision. Such repulsive potential field is formulated as

$$U_i^{(1)}(\mathbf{q}) = \begin{cases} \frac{\xi_2}{2}\left(\frac{1}{\|d(\mathbf{q}, q_i)\|_2} - \frac{1}{d_0}\right)^2, & \text{if } \|d(\mathbf{q}, q_i)\|_2 \leq d_0, \\ 0, & \text{otherwise}, \end{cases} \tag{7}$$

where ξ_2 is a positive scaling factor, $\|d(\mathbf{q}, q_i)\|_2$ denotes the distance between robot R_i that works in the states of higher or equal avoidance priority to other robots q_i that within the effective range, which values are determined by the robot dimensions.

Due to this, for any planet robot, the final constructed potential field for motion control is:

$$U_f^{(1)}(\mathbf{q}) = U_d^{(1)}(\mathbf{q}) + \sum_{i \in \mathcal{N}_{r_{vision}}^{(3,4)}} U_i^{(1)}(\mathbf{q}) \tag{8}$$

where $\mathcal{N}_{r_{vision}}^{(3,4)}$ represents robots working under *State 3 and 4* and within the vision sensing range r_{vision}.

With (8), the control input for the robot working in *State 1* is obtained:

$$\mathbf{u}^{(1)} = -\nabla U_f^{(1)}(\mathbf{q}) = \begin{cases} \xi_1(\mathbf{q}_g - \mathbf{q}) + \\ \qquad \sum_{i \in \mathcal{N}_{r_{vision}}^{(3,4)}} \left(\frac{1}{d_0} - \frac{1}{\|d(\mathbf{q}, q_i)\|_2}\right) \frac{\xi_2 \nabla d(\mathbf{q}, q_i)}{\|d(\mathbf{q}, q_i)\|_2^2}, \\ \qquad\qquad \text{if } \|d(\mathbf{q}, q_i)\|_2 \leq d_0, \\ \xi_1(\mathbf{q}_g - \mathbf{q}), \qquad \text{otherwise}, \end{cases} \tag{9}$$

where $\mathbf{u} = [u_1, u_2, ..., u_i]$ is the input velocity of all the robots under deployment. Moreover, the input velocity $\|u_i\|$ is bounded by a maximum value according to Algorithm 1.

2) Motion Controller for State 2: Similar to *State 1*, the source of attractive potential becomes the pivot robot R_{pv}, thus, we have attractive potential field formulated as

$$U_d^{(2)}(\mathbf{q}) = \frac{1}{2}\xi_3 \|d(\mathbf{q}, \mathbf{q}_{pv})\|_2^2 \tag{10}$$

where ξ_3 is a scaling parameter and $\|d(\mathbf{q}, \mathbf{q}_{pv})\|_2$ the distance between robot current positions and pivot robot.

According to the pre-decided priority for collision avoidance, the repulsive potential field for robots working in *State 2* is constructed the same as *State 1*, which results in a control law shown in (12):

$$U_f^{(2)}(\mathbf{q}) = U_d^{(2)}(\mathbf{q}) + \sum_{i \in \mathcal{N}_{r_{vision}}^{(3,4)}} U_i^{(2)}(\mathbf{q}) \tag{11}$$

$$\mathbf{u}^{(2)} = -\nabla U_f^{(2)}(\mathbf{q}) = \begin{cases} \xi_3(\mathbf{q}_{pv} - \mathbf{q}) + \\ \qquad \sum_{i \in \mathcal{N}_{r_{vision}}^{(3,4)}} \left(\frac{1}{d_0} - \frac{1}{\|d(\mathbf{q}, q_i)\|_2}\right) \frac{\xi_2 \nabla d(\mathbf{q}, q_i)}{\|d(\mathbf{q}, q_i)\|_2^2}, \\ \qquad\qquad \text{if } \|d(\mathbf{q}, q_i)\|_2 \leq d_0, \\ \xi_3(\mathbf{q}_{pv} - \mathbf{q}), \qquad \text{otherwise}. \end{cases} \tag{12}$$

3) Motion Controller for State 3: For the robot moving along $\partial\mathcal{P}$ in *State 3*, since it has no leading or trailing robot in the same state, it requires only attractive potential to motivate movement. In order to avoid a discrete control method which typically results in frequent position updates and improve control efficiency, we propose a continuous control law (13) and enable robots moving along $\partial\mathcal{P}$.

We use attractive potential (10) to motivate the movement of the robot. However, different from *State 2*, the robot in *State 3* has to move in a tangent way along $\partial\mathcal{P}$ and CCW about the pivot. Thus, we determine the control law as below:

$$\begin{gathered} \mathbf{u}^{(3)} = -T \cdot \nabla U_d^{(1)}(\mathbf{q}) = T \cdot \xi_3(\mathbf{q}_{pv} - \mathbf{q}), \\ T = \begin{bmatrix} \cos(-\pi/2) & -\sin(-\pi/2) \\ \sin(-\pi/2) & \cos(-\pi/2) \end{bmatrix} = \begin{bmatrix} 0 & 1 \\ -1 & 0 \end{bmatrix}. \end{gathered} \tag{13}$$

Particularly, it is difficult to keep the robot in the orbit and tracking $\partial\mathcal{P}$ with only attractive potential, as a disturbance may yield $\|\mathbf{q}_{pv} - \mathbf{q}\| > r_{comm}$ and break the robot connection to the pivot robot. Due to this, we can introduce an asymmetric potential function such as (26) in [12] and let $\rho_2 = r_{comm}$ and $\rho_0 = r_{\mathcal{P}j}$ for a stabilized motion.

4) Motion Controller for State 4: Since collision happens only between leading robot and its trailing robot if they are working in *State 4*, We construct an attractive potential $U_d^{(4)}$ exerted on robot R_i by its leading robot R_{i+1}. When R_i is tracking $\partial\mathcal{S}$, the measurement to the length along the spill boundary between itself and other agents within its vision sensing range is used to construct the potential field. Practically, such measurement can be performed with stereo vision sensors, LIDAR, or high resolution laser rangefinders, along with the techniques developed in [13], [14]. Suppose there is a function $s = f(\mathbf{q})$ to represent the spill boundary $\partial\mathcal{S}$, where $s \in [0, \|\partial\mathcal{S}\|]$ indicates the length between a reference point and an agent of position $\mathbf{q}$ in CCW. We can show that once a robot R_{i+1} falls within the vision range of its trailing robot R_i, the distance between the two neighboring robots, namely $l_i = \|q_i, q_{i+1}\|_{\partial\mathcal{S}}$, can be decided by

$$l_i = \begin{cases} s_{i+1} - s_i, & \text{if } s_{i+1} \geq s_i, \\ s_{i+1} - s_i + \|\partial\mathcal{S}\|, & \text{if } s_{i+1} < s_i. \end{cases} \tag{14}$$

If the leading robot of R_i is beyond its vision range r_{vision}, we define a virtual distance l_i^* and update (14) as below:

$$l_i^* = \begin{cases} l_i, & \text{if } l_i \leq r_{vision}, \\ r_{vision}, & \text{if } l_i > r_{vision} \text{ or } l_i \text{ is unknown}. \end{cases} \tag{15}$$

The attractive potential function is then defined as

$$U_d^{(4)} = \frac{1}{2}\xi_4 l_i^{*2} \tag{16}$$

where ξ_4 is a positive scaling factor. The linear velocity input u_i should be in the direction of the negative gradient of $U_d^{(4)}$ with respect to s_i such that

$$u_i^{(4)} = -\nabla_{s_i} U_d^{(4)} = \xi_4 l_i^*. \tag{17}$$

It can be easily proved that the attractive potential $U_d^{(4)}$ can motivate robot R_i to move forward and as well prevent collision with its leading robot, since it is always non-negative and $u_i \to 0 \ iff \ l_i^* \to 0$. Furthermore, all the planet robots will gather and stop around pivot robot when the coverage control is completed.

D. Coverage to the Next Packing Area

When a group of robots completes the coverage to the current packing area $\mathcal{P}_i$ and removes the spill $\mathcal{S}_i$, the pivot robot, after relocation by human operator teleoperation or navigation, can herd all the planet robots into the next packing area $\mathcal{P}_{i+1}$ to perform a new round of coverage operation. One of the practical herding strategies can be found in [15], which features robot connectivity preservation.

III. Simulation Experiments

Extensive scaled-down simulation experiments were conducted to validate the proposed collective coverage strategy in Robotarium platform [16], which is a MATLAB based open source multi-robot coordination testbed. Robotarium has a 2D arena of size 3m $\times$ 3m, where disperse scaled-down robots are deployed to simulate the collective coverage operation. A variety of scenarios were designed and tested for validation. In the experiments, R_1 denotes the pivot robot and is located at the center of the arena. The linear velocity of the robot is bounded by $v_{max} = 0.075$ m/iter. The average width d in Fig. 2a is set to be 0.33 m.

A. Evaluation Metrics

The following metrics are decided for our experiments to evaluate the performance of the proposed strategy:

1) Lyapunov candidate function (Convergence):

$$L = \sum_{R_i, R_j \in \mathcal{P}, i \neq j} \|q_i - q_j\|, \textbf{ or } L = \sum_{R_i \in \mathcal{P}} \|q_i - q_p\|. \quad (18)$$

The second function is used if only one planet robot is involved, where q_p is the location of the pivot robot.

2) The number of iterations ($k_{stop} \leq k_{max}$) to reach the following stop condition:

$$\text{Stop at } k_{stop} \text{ if the current area } A(t) \leq A_{min}. \quad (19)$$

Here A_{min} is defined to be 1% of the initial area.

B. Experiment Scenarios

The following four scenarios are designed to demonstrate the efficacy and efficiency of the proposed solution.

- *Sc. 1* - Adaptiveness to various packing shapes
- *Sc. 2* - Scalability which allows multiple robots
- *Sc. 3* - Fault tolerance to the robot with coverage failures
- *Sc. 4* - Unknown obstacle during the operation
- *Sc. 5* - Sequential coverage to multiple packing areas

All the scenarios demonstrate the convergence of the planet robots at the end of the coverage operation. The experiment videos are available at https://goo.gl/K6u589.

C. Scenario 1 - Adaptiveness to Various Packing Shapes

To demonstrate the adaptiveness to different packing shapes with our proposed collective coverage control strategy, we select four representative geometric shapes including triangle, square, hexagon, and circle. In contrast, [17] and [1] can deal with only square cell coverage.

Among all the four shapes, the circular packing method can maximize the wireless communication range, i.e., can have possibly a greater packing area with less travel of robots than other shapes. However, as the main disadvantage, circular packing allows 90.69% coverage rate with unique radius circles and hexagonal lattice arrangement [18]. To improve the coverage rate, one can use circles with different radii and increase the packing densities to be $> 91\%$ [19]. Triangular, square, and hexagonal packing methods can achieve 100% coverage rate; however, the packing shapes have to be aligned adequately to avoid overlap or gap. In practice, the alignment issue can be circumvented by assuming a uniform orientation for all packing areas using magnetic compasses. Note that $r_{\mathcal{P}j}$ in Algorithm 1 is not a constant for non-circular packing methods, hence (13) may not apply. Nevertheless, $r_{\mathcal{P}j}$ can be obtained by referencing the attitude of the pivot robot and using estimation methods such as [20].

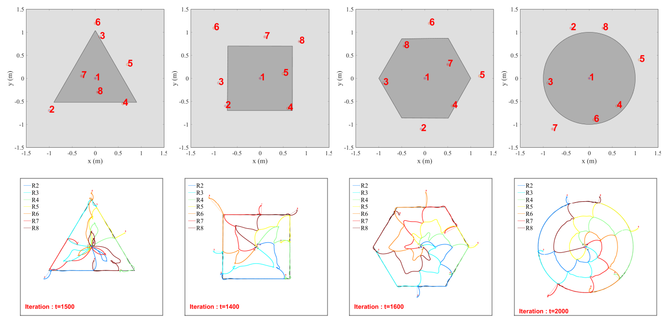

Fig. 4: The figure shows a eight-robot team performing the proposed pivot-base collective coverage over the packing areas of different shapes including triangle, square, hexagon, and circle. This robot team consists of a pivot robot, denoted as “1” and located at the centroid of the area, and seven planet robots. The planet robots are randomly distributed before the task.

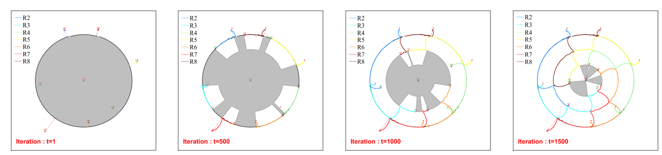

Fig. 5: The snapshots show the evolution of the robot trajectories and remaining area in shadow, under circular packing method.

The coverage performance and robot trajectories of the four packing shapes are shown in Fig. 4. One can see that a complete coverage over these areas is achieved with a eight-robot team working under our proposed control strategy. Thus, any large-scale spill which can be partitioned into several packing areas shall can be covered in the same manner. Particularly, we present area evolution snapshots for the circular packing coverage in Fig. 5, which demonstrate the evolution of robot trajectories and depict the remaining area with shadow.

Fig. 6a and 6b show the coverage performance under Situation II of Fig. 2b, where $\partial\mathcal{S}$ already exists at the beginning of the operation. In this case, robots R_5 and R_6 detected $\partial\mathcal{S}$ when continuously heading toward the pivot robot, then they entered *State 4* and started following $\partial\mathcal{S}$, rather than moving along $\partial\mathcal{P}$ as the other robots.

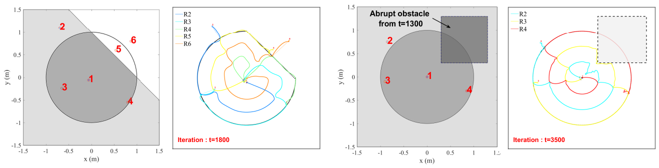

(a) (b) (c) (d)

Fig. 6: (a) Initial distribution of robots demonstrating Situation II of Fig. 2b, where $\partial\mathcal{S}$ already exists before task. (b) The trajectories of robots. (c) An abrupt obstacle was introduced during the operation in time $t = 1300_{+}$. (d) Trajectories of the robots that succeeded in avoiding the obstacle and performed complete coverage.

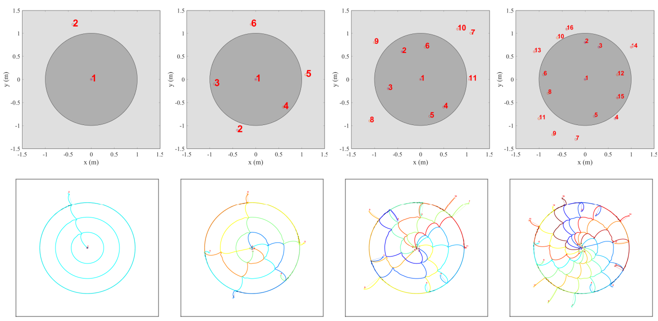

Fig. 7: The first row shows the initial random distributions of robots; the darker disk is circular packing area in the workspace. The pivot robot is 1 and located at and located at the centroid of the area. The second row shows the robot trajectories, with the amount of robots being 2, 6, 11, and 16, respectively.

D. Scenario 2 - Scalability Which Allows Multiple Robots

To improve the efficiency of coverage, we further demonstrate the scalability of our proposed solution that allows any number of planet robots. We take circular packing as an example, one can easily apply the same control scheme to other packing methods.

We start from the minimal number of robots $N = 2$, with one of them serving as pivot robot while the others being planet robots. We scale up N with the same interval of $five$ and therefore obtain four scenarios with $N = \{2, 6, 11, \text{ and } 16\}$. The initial distributions and trajectories of the robots during operation are shown in Fig. 7.

The area evolution during the cleaning process is shown in Fig. 9a, from which we conclude the improvement in the efficiency of our proposed solution. The area of the cleaning zone decreased steadily as time elapsed. The k_{stop} was reduced significantly while having more robots deployed in the cleaning operation. Nevertheless, more robots employed does not always lead to a shorter operation time. Time may be consumed in robots avoiding each other in a crowd. The results in Fig. 7 also validate the effectiveness of our robot motion controller and collision avoidance strategy by showing a smooth trajectory for every robot. The k_{stop} values for all the scenarios are listed in Table I.

At the end of the operation, all the robots gathered around the pivot robot as indicated in Fig. 7. This characteristic potentially allows further deployment such as moving to the next packing area or docking for recharging. Such convergence property is validated through Lyapunov candidate function (18) and is demonstrated in Fig. 9b. In particular, convergence in scenario $N = 2$ was step-like during operation, because the second Lyapunov candidate function in (18) was used for evaluation. While the planet robot was covering $\mathcal{P}$, it approached the pivot in an intermittent way. Additionally, due to physical restraint of robots, the Lyapunov candidate function value did not converge to *zero* when the task was completed.

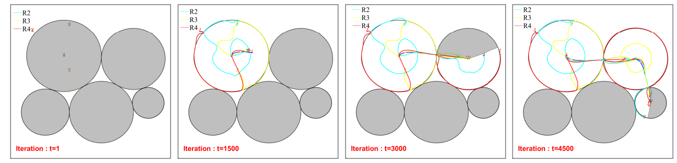

Fig. 8: The coverage evolution of a large-scale spill partially shown with snapshots using *four* robots after circular packing partition.

TABLE I: k_{stop} value and the total distance traveled by the planet robots until reaching k_{stop} for $N = 2, 6, 11,$ and 16.

Scenarios	$N = 2$	$N = 6$	$N = 11$	$N = 16$
k_{stop} *value*	7662	2247	1491	910
Distance traveled (m)	73.33	257.78	454.94	607.53

We also consider the energy consumption during the collective cleaning task, which can be reflected by the entire traveling distance of robots employed. The entire traveling distances with different N are indicated in Table I. Noticeably, at the expense of a shorter operation time, the total traveled distance increased when more robots were deployed. The evolution of traveled distance is shown in Fig. 9c.

E. Scenario 3 - Fault Tolerance to the Robot with Coverage Failures

We demonstrate fault tolerance capability of our proposed solution when the robot has coverage failure. Once employed in operation, a robot may face many issues that prevent it from removing the spill, e.g., a chemical substance removal robot facing filtering system failures, or an algae harvesting robot being fully loaded with algae. Even if the faulty robots can be simply isolated from the operation, we still want to let them converge to the pivot robot and collect them at the end of the operation, if they still have mobility.

In our experiment, the robots have the same circular packing setting demonstrated in Fig. 4. However, R_4 lost its coverage ability at $t = 500$ but regained it at $t = 1500$. Fig. 9d shows R_4 kept moving along $\partial\mathcal{S}$ and converge to the pivot robot when encountered such coverage failure. Due to this, the spill area evolution shown in Fig. 9e as the red dashline indicates a falling in the spill removal rate at $t = 500$, but it witnesses an increase at $t = 1500$ because R_4 regained the coverage ability.

F. Scenario 4 - Unknown Obstacle During the Operation

Unavoidably, the robots may encounter obstacles during the coverage operation in an unknown environment, such as rocks in water areas and robots that lose mobility. We demonstrate the capability of our strategy in abrupt obstacle

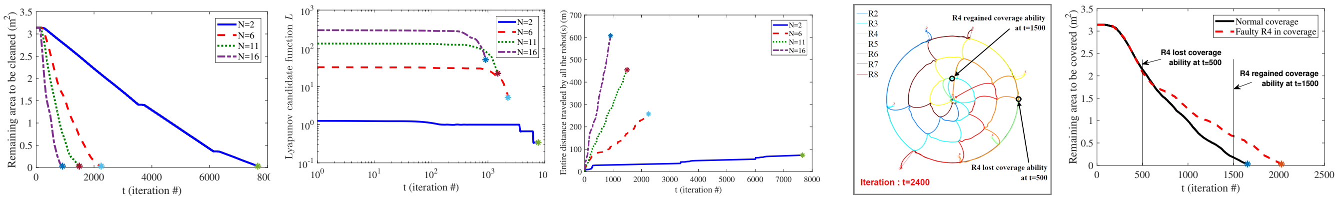

(a) (b) (c) (d) (e)

Fig. 9: (a) The area evolution of the packing area as time elapsed, starting from the initial value of 3.14. The star sign at the end of every line indicates the k_{stop} value of the corresponding scenario. (b) The convergence of the robot team in logarithmic while the task is performed. The star sign at the end of every line indicates k_{stop} of the corresponding scenario. (c) The distance traveled by all the working robots while performing the cleaning task. (d) R_4 encountered a coverage failure at $t = 500$ when moving along ∂S but recovered at $t = 1500$. It still converged to the pivot robot at the end. (e) The area evolution when R_4 was with (red) and without (black) a failure.

avoidance. As shown in Fig. 6c, an abrupt obstacle was introduced in time $t = 1300_+$; however, the robot team succeeded in avoiding this obstacle using approaching sensors such as sonars and LIDARs, and achieved complete coverage over the area still, as shown in Fig. 6d.

G. Scenario 5 - Sequential Coverage to Multiple Areas

We demonstrate a large spill coverage scenario using *four* robots after partition with circular packing as described in Sec. II-D. The large spill was removed in sequence by covering every individual packing area, which process is partially depicted with snapshots in Fig. 8 due to space limit.

IV. Conclusion and Future Work

In this paper, a novel pivot-based collective coverage strategy with a multi-robot team is proposed for large-scale spills coverage problems. The proposed strategy is validated through simulation experiments to be adaptive to various packing areas and can achieve a complete coverage, and further realizes the cleanup to the large-scale spill by covering all the partitioned packing areas in sequence. With the proposed solution, all planet robots will converge to the pivot robot at the end of the operation, which enables further operations such as cleaning up the next partition area, docking for recharging, etc. This collective coverage strategy features strong capabilities including scalability, fault tolerance to coverage failures, and abrupt obstacle avoidance, which further enhance its efficiency and robustness. Our future goals mainly focus on validating our solution with field tests, and promoting collaboration among multiple teams.

References

[1] X. Jin and A. Ray, "Navigation of autonomous vehicles for oil spill cleaning in dynamic and uncertain environments," *International Journal of Control*, vol. 87, no. 4, pp. 787–801, 2014.

[2] M. A. Batalin and G. S. Sukhatme, "Coverage, exploration and deployment by a mobile robot and communication network," *Telecommunication Systems*, vol. 26, no. 2-4, pp. 181–196, 2004.

[3] A. Breitenmoser and A. Martinoli, "On combining multi-robot coverage and reciprocal collision avoidance," in *Distributed Autonomous Robotic Systems*, pp. 49–64, Springer, 2016.

[4] J. A. Bennell and J. F. Oliveira, "A tutorial in irregular shape packing problems," *Journal of the Operational Research Society*, vol. 60, no. sup1, pp. S93–S105, 2009.

[5] B.-C. Min, E. T. Matson, and J.-W. Jung, "Active antenna tracking system with directional antennas for enhancing wireless communication capabilities of a networked robotic system," *Journal of Field Robotics*, vol. 33, no. 3, pp. 391–406, 2016.

[6] B.-C. Min, R. Parasuraman, S. Lee, J.-W. Jung, and E. T. Matson, "A directional antenna based leader–follower relay system for end-to-end robot communications," *Robotics and Autonomous Systems*, vol. 101, pp. 57–73, 2018.

[7] E. Montijano, E. Cristofalo, D. Zhou, M. Schwager, and C. Saguees, "Vision-based distributed formation control without an external positioning system," *IEEE Transactions on Robotics*, vol. 32, no. 2, pp. 339–351, 2016.

[8] J. Fink and V. Kumar, "Online methods for radio signal mapping with mobile robots," in *Robotics and Automation (ICRA), 2010 IEEE International Conference on*, pp. 1940–1945, IEEE, 2010.

[9] MIT Senseable City Lab. http://senseable.mit.edu/seaswarm/. Accessed: July 31, 2018.

[10] T. Weerakoon, K. Ishii, and A. A. F. Nassiraei, "An artificial potential field based mobile robot navigation method to prevent from deadlock," *Journal of Artificial Intelligence and Soft Computing Research*, vol. 5, no. 3, pp. 189–203, 2015.

[11] S. Makris, G. Michalos, and G. Chryssolouris, "Rfid driven robotic assembly for random mix manufacturing," *Robotics and Computer-Integrated Manufacturing*, vol. 28, no. 3, pp. 359–365, 2012.

[12] M. M. Zavlanos, M. B. Egerstedt, and G. J. Pappas, "Graph-theoretic connectivity control of mobile robot networks," *Proceedings of the IEEE*, vol. 99, no. 9, pp. 1525–1540, 2011.

[13] S. Gowal, A. Prorok, and A. Martinoli, "Two-phase online calibration for infrared-based inter-robot positioning modules," in *Intelligent Robots and Systems (IROS), 2011 IEEE/RSJ International Conference on*, pp. 3313–3319, IEEE, 2011.

[14] A. Mitiche and J. K. Aggarwal, *Computer vision analysis of image motion by variational methods*. Springer, 2014.

[15] R. Parasuraman, J. Kim, S. Luo, and B.-C. Min, "Multipoint rendezvous in multirobot systems," *IEEE transactions on cybernetics*, 2018.

[16] D. Pickem, P. Glotfelter, L. Wang, M. Mote, A. Ames, E. Feron, and M. Egerstedt, "The robotarium: A remotely accessible swarm robotics research testbed," in *Robotics and Automation (ICRA), 2017 IEEE International Conference on*, pp. 1699–1706, IEEE, 2017.

[17] J. Song, S. Gupta, J. Hare, and S. Zhou, "Adaptive cleaning of oil spills by autonomous vehicles under partial information," in *Oceans-San Diego, 2013*, pp. 1–5, IEEE, 2013.

[18] H.-C. Chang and L.-C. Wang, "A simple proof of thue's theorem on circle packing," *arXiv preprint arXiv:1009.4322*, 2010.

[19] A. Heppes, "Some densest two-size disc packings in the plane," *Discrete & Computational Geometry*, vol. 30, no. 2, pp. 241–262, 2003.

[20] P. Narkhede, A. N. Joseph Raj, V. Kumar, V. Karar, and S. Poddar, "Least square estimation-based adaptive complimentary filter for attitude estimation," *Transactions of the Institute of Measurement and Control*, pp. 1–11, 2018.